I. Introduction

It is claimed that life would not be possible without radioactivity, which is an essential component of life. Life on Earth began when naturally occurring radioactivity heated the Earth's core [**?**]. The science of radioactivity has come a long way since Henri Becquerel discovered it in 1896, and it is now a prerequisite for many modern technologies. Radioactive elements are used in scientific studies to determine the age of rocks and fossils. For example, radioactive materials are employed in health imaging and disease treatment. In energy, radioactive materials are utilized in nuclear power plants and spacecraft.

However, the inherent properties of radioactive materials that make them valuable also present significant challenges in handling and security. These materials are invisible to the naked eye and can be easily concealed, making their detection and tracking a complex technological challenge. The risks associated with radioactive materials are compounded by their potential for malicious use, whether as weapons or as a means of environmental contamination.

A. Motivation

It is essential to develop trustworthy techniques for locating radioactive sources. First, these methods can significantly enhance security measures by helping law enforcement and security agencies spot possible threats faster. Second, quick detection of radioactive leakage is essential for preserving operational safety and safeguarding the environment and employees in industrial settings such as nuclear power plants. Localizing radioactive sources is intriguing yet challenging, highlighting the need for continued research. Strong simulation frameworks are required since testing with actual radioactive sources can be dangerous and complicated by nature. Furthermore, comprehending the complex physical behavior of radiation, particularly particle attenuation and scattering, presents intriguing modeling problems that affect simulations' accuracy and localization's efficacy. Although various methods have been put forth, they are less feasible for rapid source detection because they are computationally intensive and necessitate broad area searches. It is very important to have a set of tools and methods that can effectively localize the radiation source without human interference, as the need for this is very relevant in recent times. This way, we can ensure public safety and environmental protection.

B. Problem Statement

The fundamental challenge in radioactive source localization lies in using sensor measurements and prior knowledge to estimate the position and intensity of unknown radiation sources within an environment. Current approaches face several key limitations: they often require an exhaustive and complete search of the entire search area, struggle with sensor noise and measurement uncertainty, perform poorly in environments with limited accessibility, and suffer from high computational complexity when dealing with dynamic and large search spaces.

The core research problem encompasses three main aspects. First, the development of a physics-accurate simulation framework that can reliably model radiation behavior, including particle attenuation and scattering effects. Second, a comprehensive evaluation framework capable of assessing and comparing different localization approaches must be created. Third, the implementation and analysis of various localization algorithms, examining their computational complexity, resource requirements, accuracy, and efficiency across different environmental conditions.

Despite advances in radiation source localization, existing methods often rely on simplified models that inadequately capture real-world radiation physics and lack systematic ways to compare different approaches. Current solutions frequently compromise detection speed and computational efficiency, limiting their practical application.

Our research addresses these challenges through three key contributions: the development of a physics-accurate simulation framework incorporating realistic radiation behavior, the implementation of three complementary localization algorithms (information-gain-based, rollout-based, and inverse square optimization), and the establishment of a comprehensive evaluation methodology. Together, these contributions enable a detailed comparison of the implemented algorithms given the chosen metrics, advancing the field toward more practical and efficient solutions.

We present a framework that integrates simulation, evaluation, and algorithm implementation to tackle these challenges. The simulation component uses established radiation physics models to create realistic test scenarios, incorporating inverse square law, attenuation, and scattering effects. The evaluation framework provides quantitative metrics for assessing algorithm performance, including computational efficiency, accuracy, and robustness to noise. We implement and compare several localization methods, including rollout algorithms, entropy-based approaches, and optimization-based methods. Each method is systematically evaluated under various environmental conditions and constraints. We aim to develop an integrated system that allows for robust and flexible implementation and testing of various radiation source localization algorithms.

II. Related Work

The subject of radioactive source localization has not been explored as extensively as other localization problems. The main characteristic of the radioactive source search is about controlling the observer(s) position. The related works in the context of radioactive source localization have proposed different methods to solve the problem. Traditional methods relied heavily on using a high number of sensors in the search and then localizing the estimated source position using the least squares method [**?**] [**?**]. In the conventional methods, the observer moves through the search area following a predefined path [**?**]. Such a method was proposed by using uniform search [**?**]. Some of these autonomous methods use triangulation-based techniques to localize the source [**?**] [**?**]. These conventional methods, while functional, face several critical limitations in efficiently localizing radioactive sources. Static

sensor networks and predefined search path approaches require extensive coverage of the search area, making them more time-consuming and computationally expensive. As noted in recent studies, traversal-based methods, though accurate, suffer from extremely low search efficiency [**?**]. These methods become highly unreliable with larger search areas as they lack the intelligence to adapt to the environment.

Bayesian estimation is a commonly used method in the context of radioactive source localization. These methods are widely adopted due to their ability to handle uncertainties and incorporate prior information in the localization process [**?**]. According to the Bayesian criterion, the localization of an unknown radioactive source can be determined by solving the posterior probability distribution of the source parameter vector, which can be represented through various methods, including the particle filter [**?**] [**?**] [**?**] and other probabilistic methods. The particle filter-based method, Ling et al. [**?**] highlight that the particle filter stands out as a practical approach that approximates the posterior distribution by maintaining and iteratively updating a set of weighted particles. At each step, the particles' weights are updated based on how likely the observed measurements are under each particle's hypothesis, and low-likelihood particles are replaced by higher-likelihood ones. As shown by Ristic et al. [**?**], this resampling process helps to maintain particle diversity while converging towards the most likely source parameters. They extended the particle filter approach further by introducing the information-driven strategy. Their method combines sequential Bayesian estimation with Fisher information-based observer control to optimize measurement collection. Initially, when source detection confidence is low, the observer moves through the search area following an exploration pattern. After the detection threshold is reached with sufficient probability, the observer's motion and exposure time are controlled to maximize the information gain of future measurements. This method helps to guide the observer to positions that are expected to provide the most information about the source parameters. However, a key limitation of fisher information that emerged in the study of Ristic et al. [**?**] is that it cannot be used before the source detection. To overcome this limitation, Ristic et al. proposed a method that uses Rényi divergence between current and predicted future posterior densities as the information gain metric. This Rényi divergence enables observer control even before the source detection by considering the complete probability density function rather than just parameter estimates. This allows for more optimal data collection and observer control, leading to faster and more accurate source localization even before the source is detected.

Rollout algorithms, introduced by Bertsekas, represent a sequential optimization approach where variables are optimized one after another. Starting with a base policy or heuristic, rollout algorithms construct an improved policy through a one-step lookahead, often yielding significantly better performance than the original heuristic while maintaining implementation simplicity [**?**]. Several researchers have explored rollout algorithms for source localization and path planning. Hoffmann et al. proposed a rollout-based path planner that optimizes mobile sensor trajectories for RF source localization using lookahead policies and cost-based optimization. While their focus was on RF sources, the approach is generalizable to other source types, including radioactive sources, due to their similar signal characteristics [**?**]. Tian et al. developed a multi-step lookahead policy for UAV surveillance that incorporates a layered decision framework to balance multiple objectives, including safe navigation and target tracking. Their work demonstrates the effectiveness of rollout policies in anticipating future states and making informed decisions for path planning tasks [**?**]. These works demonstrate the potential of rollout algorithms for efficient path planning and source localization. The success of Hoffmann et al.'s approach with RF sources and Tian et al.'s implementation for UAV surveillance suggests that adapting rollout mechanisms shows significant potential for radiation source localization. The method's ability to improve upon base heuristics while maintaining computational efficiency makes it especially suitable for radiation scenarios where quick localization is crucial. Furthermore, the one-step lookahead policy could help navigate the complex radiation fields while accounting for particle attenuation and scattering effects.

III. Methodology

A. Simulation Framework

A set of simulation frameworks was investigated to select the best simulation that is available for the project. Gazebo was selected as the simulation based on its compatibility with ROS2 and the availability of the plugins that are already made available due to the familiarity of the platform. The SJTU drone system was selected as the drone model for the simulation as it was lightweight and also easy to work with. A new radiation sensor plugin and radiation source plugin were developed to simulate the radiation source and the sensor. This plugin can be easily integrated into the simulation and can be used to simulate the radiation source and the sensor.

To accurately represent realistic radiation behavior, the radiation source is modeled as a point gamma radiation source that emits radiation uniformly in all directions. The system transforms raw radiation activity (measured in Becquerel per square meter), which is derived by applying the inverse square law. This fundamental physical principle describes how radiation intensity decreases quadratically with distance from the source, allowing precise calculation of radiation density at varying distances. The system converts this distance-dependent surface activity into a photon count rate by multiplying the intensity with detector-specific parameters, including active area, gamma emissions per decay, detector efficiency, and fractional live time. A Poisson distribution is then applied to simulate the probabilistic nature of radiation detection, generating a statistically realistic representation of radiation measurement.

The radiation sensor receives and publishes data in the form of photon count rates; however, this count rate is subject to attenuation caused by trees and the air surrounding the sensor.

The attenuation from trees is implemented through ray tracing, which helps to determine if the sensor has a clear line of sight to the radiation source. If trees obstruct the line of sight, the radiation is attenuated based on the type of tree

and a specific attenuation factor. The positions of the trees are generated dynamically according to the map size while ensuring a maintained specific distance between each tree.

B. Evaluation Framework

A new interface for handling the simulation and experiment metrics was developed. The interface is designed with PyQt5, a Python library for creating graphical user interfaces. Two interfaces have been developed that allow one to either handle all the parameters in the workspace or visualize any number of algorithms running within the workspace.

1) Parameter Editor: The parameter editor application serves multiple purposes beyond the current project. It was developed to provide a unified interface that consolidates all configuration files in YAML format. To ensure compatibility with ROS2 packages, the interface can load the names of the ROS2 packages of interest from a YAML file. This file is then processed to identify which packages should be searched for within the root of the ROS2 workspace. The identified YAML files are sorted according to the package or workspace in which they were found, allowing the user to select the package of interest. Once selected, the YAML files are loaded and displayed in a tabular format. This interface enables the users to add, remove and, save changes to the YAML files.

Another feature of this interface is its ability to identify common parameters shared across different algorithms. These parameters can include the search area, source location, ROS2 topic names, and more. Changes made in this section of the application are applied to all instances of the same parameters across the project workspace. This functionality enables users to transition or migrate the project to different simulation frameworks or configurations with varying parameters.

2) Evaluation Visualizer: The results of each algorithm, upon successful completion, is saved in a standardized JSON file format. All metrics contained in these files are consistent across all algorithms, which facilitates easier comparison and visualization of the results.

The Evaluation Visualizer is an interface designed to visualize these results based on a set of configurations. When the interface is opened, the user can select the input directory containing the saved JSON files, followed by a directory where the evaluated files will be saved. Once the input directory is selected, the interface loads all JSON files and categorizes them by algorithm name. From this interface, users can specify the number of experiments to be evaluated from the total runs. After processing the analysis, the results of the algorithm runs are evaluated and displayed in the next tab, with a copy saved locally for future visualization.

The algorithms are assessed together based on predefined performance metrics, and various plots representing additional metrics from the runs are generated along with a report that tabulates the evaluation results for each algorithm.

This interface also comes with an extra tab that gives the option to generate different types of plots based on the metrics that can be selected for both the x and y-axis. The corresponding plot will be generated and displayed within the same window.

This application additionally provides a feature to do statistical analysis of the results. The users can select the metrics they want to perform the analysis on, and this will generate a statistical analysis report that can be read and interpreted by the user.

C. Algorithms

In this section, we describe the three algorithms that were implemented for the radiation source localization problem. The algorithms are based on different strategies and approaches to localize the radiation source. In rollout-based and information gain-based methods, the drone follows a shamrock pattern until source detection, after which it switches to the respective exploitation methods. The shamrock pattern serves as a systematic exploration strategy, featuring four distinct petals that emanate from the center of the search area. The drone begins at the central point and traverses the pattern in an anticlockwise direction. This pattern is particularly effective for radiation source detection for several reasons. The shamrock pattern ensures overlapping in some parts of the trajectory along the petals, ensuring no significant gaps in the search area. The radial nature of the pattern always keeps the drone referenced to the center of the search area, thereby enabling efficient coverage.

1) Information-Gain-based Algorithm: The proposed method combines a particle filter for sequential Bayesian estimation with information-driven observer control using Rényi divergence. The particle filter approximates the joint posterior density of the source parameters through a set of weighted particles, while Rényi divergence guides measurement collection to maximize information gain. This method operates in two distinct phases: an initial exploration phase and an information-driven exploitation phase. Unlike previous approaches that use Fisher information for observer control after detection [**?**], this method uses Rényi divergence throughout both phases. This choice is motivated by the ability of Rényi divergence to enable optimal measurement collection by considering the complete probability density function rather than just parameter estimates.

a) Particle Filter Framework: The source state $X = [x, y, I]^T$ comprises 2D position (x, y) and intensity I following the established approach from Ristic et al. who demonstrated that a 2D formulation for ground-based radiation sources is both effective and computationally efficient. While radiation physically propagates in 3D space, the measurement model can be effectively simplified to 2D since the height difference between source and detector remains constant and does not contribute additional information for horizontal localization. The posterior distribution is approximated using weighted particles:

$$p(X|z_{1:k}) \approx \sum_{i=1}^{N} w_k^i \delta(X - X_k^i) \tag{1}$$

where X is the radiation source state vector containing position (x, y) and intensity I, $z_{1:k}$ represents all measurements up to time k, w_k^i is the normalized weight of particle i, N is the total number of particles, $\delta(\cdot)$ is the Dirac delta function,

X_k^i is the state vector of the i^{th} particle at time k containing hypothesized source location (x_k^i, y_k^i) and intensity I_k^i.

b) Particle Initialization: The particles are initialized uniformly across the search area with a total particle count of $N(5000)$. These are distributed as follows, Position components (x,y) are initialized on a uniform grid covering the search area with additional random positions if needed. Intensity values are initialized between 5000 and 15000 Bqs to cover a wide range of possible source intensities. The particle weights are initialized uniformly as $w_0^i = 1/N$. The choice of particle count is based on the trade-off between computational efficiency and estimation accuracy. A higher particle count may provide more accurate convergence, but it may lead to increased computational complexity and slower convergence. A smaller particle count may lead to faster computation but may result in less accurate estimates. Considering these factors, along with the necessity to maintain diverse particles in the search area, a particle count of 5000 was selected as a reasonable compromise.

The radiation measurement model incorporates inverse square law decay and atmospheric attenuation:

$$\lambda(X, x_k) = \left(\frac{I}{d^2(x_k, X)} + \mu_b \right) \tau_k \cdot \exp(-\beta d(x_k, X)) \quad (2)$$

where, $\lambda(X, x_k)$ is the expected measurement rate at position x_k, I is the source intensity, $d(x_k, X)$ is the distance from measurement position to source, μ_b is the background radiation rate, τ_k is the measurement exposure time, β is the atmospheric attenuation coefficient.

c) Two-Phase Search Strategy: The source is present in search area as a point source emitting gamma radiation. While the radioactive source is present throughout the experiment, the detection refers to the algorithm's statistical confidence that measurements indicate a radioactive source is distinguishable from background radiation. To find this distinguishable confidence, the algorithm operates in two distinct phases: exploration and exploitation. During the exploration phase, the detection probability is monitored using:

$$P(\text{detection}|z_k) = \frac{r_k}{1 + r_k}, \quad r_k = \frac{\frac{1}{N}\sum_{i=1}^{N} P(z_k|X_k^i)}{P(z_k|\text{background})} \quad (3)$$

where, $P(\text{detection}|z_k)$ is the probability of source presence, r_k is the likelihood ratio, $P(z_k|X_k^i)$ is the measurement likelihood for particle i, $P(z_k|\text{background})$ is the background-only likelihood. The detection strategy uses a sliding window of the last 5 calculated probabilities and terminates when the three consecutive probabilities exceed the detection probability threshold of 0.95. This is done to ensure that the triggered detection is reliable and not a false positive.

In the exploitation phase, measurement locations are optimized using Rényi divergence:

$$D_\alpha(x'_k) = \frac{1}{\alpha - 1} \log \left(\frac{g_\alpha(x'_k)}{g_1(x'_k)^\alpha} \right) \cdot E(x'_k) \quad (4)$$

with:

$$g_\alpha(x'_k) = \frac{1}{N} \sum_{i=1}^{N} \exp(\alpha \hat{z}_k^i) \quad (5)$$

where, $D_\alpha(x'_k)$ is the Rényi divergence for candidate position x'_k, α is the Rényi divergence parameter ($\alpha > 0$), $\hat{z}_k^i$ is the predicted measurement at position x_k for particle i. which was then normalized for numerical stability Then $g_\alpha(x'_k)$ combines these normalized predictions into a weighted sum, where α controls how much weight is given to larger predictions, $E(x'_k)$ is the exploration bonus term. The primary distinction between our approach and Ristic et al. [**?**] lies in the modification of the Rényi divergence calculation. While maintaining the same core information-theoretic framework, we introduce an exploration bonus term $E(x'_k)$ that explicitly rewards measurements in areas of low particle density. This modification helps balance the exploitation of high-information regions with the exploration of uncertain areas, potentially leading to more robust source localization. The original formulation by Ristic et al. focused purely on information gain, which could sometimes lead to overly concentrated measurements around the estimated source position.

Rényi divergence generalizes mutual information and provides a measure of how well a candidate measurement position x'_k can distinguish between the current posterior distribution of the source state and a uniform or background distribution.

d) Sequential State Estimation: The particle weights are updated using:

$$w_k^i = \frac{\tilde{w}_k^i}{\sum_{j=1}^{N} \tilde{w}_k^j} \quad (6)$$

with unnormalized weights:

$$\tilde{w}_k^i = w_{k-1}^i \cdot \exp(\log L_k^i - \max_j \log L_k^j) \cdot c_k^i \quad (7)$$

where, w_k^i is the normalized weight of particle i at time k, $\tilde{w}_k^i$ is the unnormalized weight, L_k^i is the measurement likelihood for particle i, c_k^i is the geometric consistency term. The geometric consistency term c_k^i evaluates how well each particle explains the measurement patterns obtained from different observation angles, complementing the circular measurement strategy used for position selection. This is implemented by tracking the last three measurement positions and computing the standard deviation of distances between each particle and these positions. Particles that maintain consistent distances across multiple measurement angles receive higher weights through an exponential weighting function. This circular measurement pattern is particularly significant as demonstrated by Ristic et al. [**?**], who in their first method showed that measuring in a circle around the estimated source position helps discriminate the true source location, since getting too close to the source can result in higher measurement uncertainty and estimation errors. To maintain particle diversity, resampling occurs when the effective sample size ($N_{eff} = 1/\sum_i (w_k^i)^2$) falls below $N/3$. The strategy preserves 30% of highest-weight particles and systematically resamples the remainder. Gaussian noise is then applied with a gradual factor of 0.7 to prevent particle collapse while ensuring smooth convergence. The algorithm's convergence is determined through multiple criteria that must be simultaneously satisfied for 8 consecutive measurement updates which were decided with multiple tests. These criteria are: the particle spread must be less than

1.0m in both spatial dimensions, while the estimated source position must remain stable within 0.5m variation across the last 10 estimates. These conservative termination conditions help reduce premature convergence or false positives while ensuring robust source localization.

This framework enables efficient source detection and localization by combining systematic exploration with information-driven measurement optimization. The particle filter handles the non-linear measurement model while maintaining uncertainty estimation throughout the process.

Figure 1 illustrates the workflow of the information gain-based algorithm, highlighting the transition from shamrock pattern exploration to information-driven exploitaion using Rényi divergence.

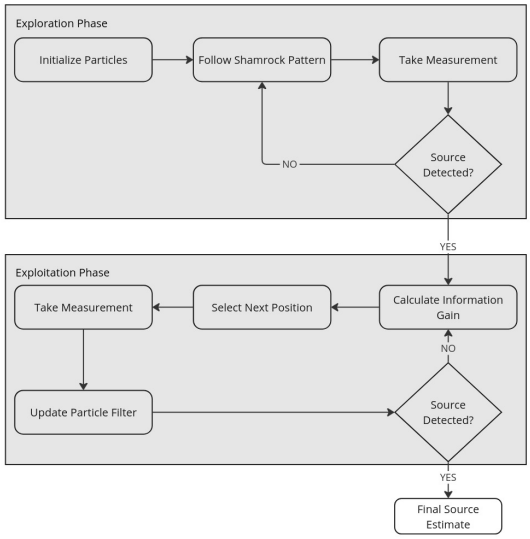

Fig. 1: Diagram showing the two-phase particle filter-based source localization process: exploration using shamrock pattern followed by information-driven exploitation using Rényi divergence

Figure 2 represents the run of the information gain-based radiation source localization algorithm for a source located at (30, 50). The particles are uniformly distributed across the search area initially, and the algorithm converges on the true source location after the source has been detected using 3 starting from figure 2.b. The final source location theoretically is the point where the particles converge as in figure 2.d.This run localized the source at a distance of 3 meters from the actual source location.

2) Rollout-based Algorithm: The algorithm operates in two primary phases: an initial systematic exploration using a shamrock search pattern, followed by an information-driven exploitation phase where the drone uses rollout-based path planning to efficiently converge on the radiation source's location. By simulating multiple potential paths and evaluating them through a sophisticated value function, the algorithm aims to optimize the trade-off between gathering immediate information and maintaining comprehensive search coverage.

a) Belief update methodology: The core of this method is the belief update mechanism that transforms the radiation measurements into a probabilistic representation of the source's

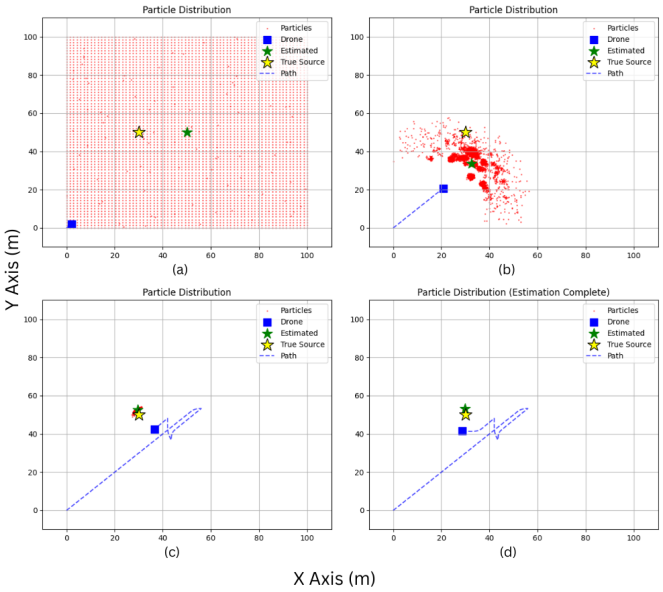

Fig. 2: Information gain-based radiation source localization for source location (30, 50): a. Initial particle distribution across search area, b. Particle resampling when source is detected with high probability using equation 3, c. Convergence of particles near true source location, and d. Final source position estimation with completed path

potential location. This belief update method employs a three-dimensional grid-based representation of the search area, with each grid cell containing a probability value that represents the likelihood of the source being located. For a typical search area of 100 x 100 meters, a grid resolution of 5 meters was selected to balance computational efficiency with localization accuracy. When the grid resolution is too fine, the algorithm may struggle to converge due to the higher number of grid cells, while a coarser resolution may lead to higher prediction error.

The belief update process begins with computing the likelihood of each measurement given potential source configurations. For a measurement m_i at the drone's position, the likelihood of the measurement given a hypothesized source at position x_j with intensity I_k is modeled as:

$$L(m_i|\mathbf{x}_j, I_k) = \frac{1}{\sqrt{2\pi\sigma^2}} \exp\left(-\frac{(m_i - \hat{m}(\mathbf{x}_j, I_k))^2}{2\sigma^2}\right) \quad (8)$$

Here, σ represents the measurement uncertainty, which scales proportionally with the expected measurement intensity: $\sigma = 0.5 \cdot \hat{m}(\mathbf{x}_j, I_k)$. $\mathbf{x}_j$ represents a vector containing the hypothesized source position coordinates and denoted as $\mathbf{x}_j = (x_j, y_j)$. This scaling captures the physical reality that measurement noise increases with radiation intensity. The measurement model from entropy algorithm is different from what is used in the rollout algorithm. The measurement model in equation 2 as it is based on the works on the works of ristic et al. The measurement model in rollout algorithm is used as

a simple measurement model to construct a probabilistic grid-based representation of the search area.

The expected measurement $\hat{m}(\mathbf{x}_j, I_k)$ is computed using the inverse square law for radiation propagation, incorporating the drone's height h for accurate distance calculations:

$$\hat{m}(\mathbf{x}_j, I_k) = \frac{I_k}{(x - x_j)^2 + (y - y_j)^2 + h^2} \tag{9}$$

Where (x, y) represents the drone's position, (x_j, y_j) represents a potential source location, and I_k is the hypothesized source intensity. This equation reflects how radiation intensity decreases with the square of the distance from the source, just as light spreads out from a point source.

The system updates its belief state using Bayes' rule, which combines the likelihood of new measurements with prior beliefs. Let m_i represent the radiation intensity measurement (count rate) obtained at the drone's current position:

$$P(\mathbf{x}_j, I_k | m_i) = \frac{P(m_i | \mathbf{x}_j, I_k) P(\mathbf{x}_j, I_k)}{\sum_{j,k} P(m_i | \mathbf{x}_j, I_k) P(\mathbf{x}_j, I_k)} \tag{10}$$

Where $P(\mathbf{x}_j, I_k | m_i)$ is the posterior probability over position and intensity, $P(m_i | \mathbf{x}_j, I_k)$ is the measurement likelihood, and $P(\mathbf{x}_j, I_k)$ is the prior probability.

The belief confidence, which is crucial for detection and convergence checking, is calculated as the maximum posterior probability across all grid cells and intensities:

$$\text{confidence} = \max_{j,k} P(\mathbf{x}_j, I_k | m_i) \tag{11}$$

The algorithm uses this confidence measure, along with several other important metrics, to make key decisions about source detection and convergence. During the exploration phase, source detection is determined through three key criteria that work together. First, the belief confidence must exceed 0.50, indicating a reasonable level of certainty in the source location. Second, the system must have collected at least five measurements to ensure sufficient data for reliable detection. Third, the algorithm checks for stability in the source position estimate - specifically, the maximum likelihood estimate of the source position must not change by more than 5 meters between consecutive updates. This stability check helps prevent false detections due to temporary measurement anomalies.

The final convergence requirements are noticeably stricter and are intended to guarantee high-confidence radiation source localization. The source location estimate must be extremely certain, as the belief confidence threshold is increased to 0.95. To ensure that the final estimate is supported by a solid dataset, the minimum number of measurements is doubled to ten. The position estimate's stability requirement is raised by the requirement that the maximum likelihood estimate remain within two meters of its previous value. The drone must be within two meters of the estimated source location, according to the algorithm's additional requirement for physical proximity. This proximity criterion is particularly important since it allows the system to acquire high-quality, last-minute measurements up close, which is crucial for verifying the source location estimate.

b) Rollout Implementation: The rollout algorithm in dynamic optimization problems represents a form of approximate dynamic programming that uses a base heuristic through lookahead and policy iteration [**?**]. A rollout algorithm simulates multiple trajectories that represent possible future states from the current state, uses the base heuristic to evaluate these trajectories, and chooses the action that maximizes the objective. This algorithm was implemented for the localization of radioactive sources by guiding the UAV to utilize a rollout-based path planning strategy to select the next best position to move. This algorithm borrows concepts and observations from previous works by Hoffmann et al. [**?**] and Tian et al. [**?**]

While Hoffmann et al. focused on bearing only RF emitter localization, the approach for radiation source localization needed some adaptations as it had to account for the challenges in localizing radiation sources. Where the original work focussed on optimizing bearing measurements and movement costs, our approach needed to account for radiation characteristics such as inverse square law decay, intensity estimation, and radiation attenuations. The intensity estimation is relevant here as the algorithm does not have prior knowledge of the source intensity. Hoffmann et al. use a Q-value $Q(s, a)$, which is basically the expected cumulative reward of taking action in state s and following an optimal policy thereafter. In their work, The Q-value is estimated by considering the immediate cost, combining movement and measurement time, and the expected future cost, which is again considered the movement and measurement time.

To adapt the Q-value computation for radiation-specific physics and simulated radiation measurements, the following modifications were done:

$$Q(s_t, a_t) = \sum_{t=0}^{T} \gamma^t V(s_t, m_t) \tag{12}$$

where $V(s_t, m_t)$ is the value function combining belief values and simulated radiation measurements:

$$V(s_t, m_t) = \frac{\sum_{i,j \in M} b(i,j)}{1 + d(s_t, x_{i,j})} + \frac{1}{1 + 0.2 * d\_max} \tag{13}$$

where m_t is the simulated measurements at time t, $\gamma = 0.9$ is the discount factor, $b(i, j)$ is the belief at grid cell (i, j), s_t represents the state (drone position and belief) at time t, and a_t represents the action (movement) being evaluated, $d(s_t, x_{i,j})$ is the distance from state s_t to grid cell (i, j), d_max is the distance to the maximum belief point, T is the planning horizon representing how many steps to look ahead and M represents the set of grid cells within the search area boundaries. The discount factor γ helps balance between immediate and future rewards, ensuring that the cumulative reward does not grow unbounded and thereby making the comparison between trajectories more meaningful. Furthermore, the discount factor helps to retain the focus on early rewards in the trajectory than later, as it may contain crucial information that can guide the estimation. The denominator terms in the value function creates an inverse relationship where positions closer to high belief area gets higher values,

and the 0.2 coefficient is used to make this proximity bonus more gradual than the belief bonus.

To evaluate these Q-values in practice, the rollout algorithm performs trajectory planning by generating multiple candidate trajectories from the drone's current position. At each decision point, the algorithm calculates a set of possible movement angles based on the current belief state and drone position, after which the algorithm simulates multiple potential paths with adaptive step sizes. Each simulated path allows the algorithm to compute the corresponding Q-value by evaluating the value function along the trajectory, accounting for both immediate measurement potential and future exploration value. This systematic evaluation of possible trajectories through Q-value computation allows the system to make decisions that balance the immediate need for information with the strategic value of maintaining efficient coverage of the search area.

The exploitation phase continues until strict convergence criteria are met: the belief confidence must exceed 0.95, the maximum likelihood estimate must remain stable across multiple measurements, and the drone must confirm proximity to the estimated source location through direct measurements. This systematic evaluation of possible trajectories through Q-value computation allows the system to make decisions that balance the immediate need for information with the strategic value of maintaining efficient coverage of the search area.

Figure 3 illustrates the workflow of the rollout algorithm demonstrating how the belief map update mechanism integrates with the Q-value computation for rollout trajectory selection

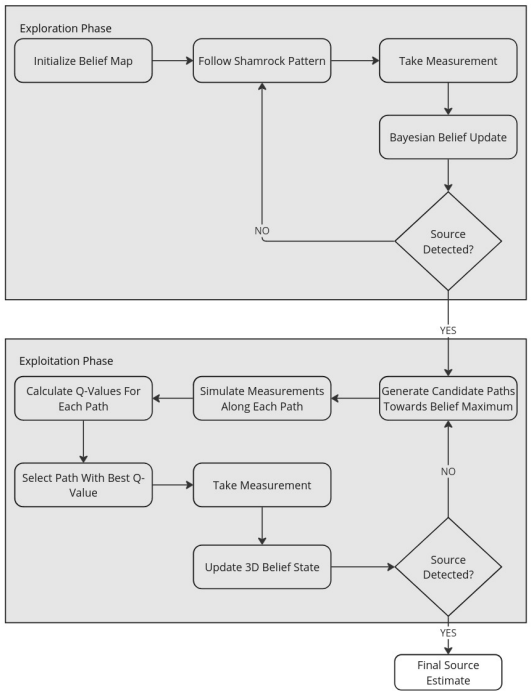

Fig. 3: Diagram illustrating the belief update and Q-value based decision process, transitioning from shamrock exploration to trajectory optimization

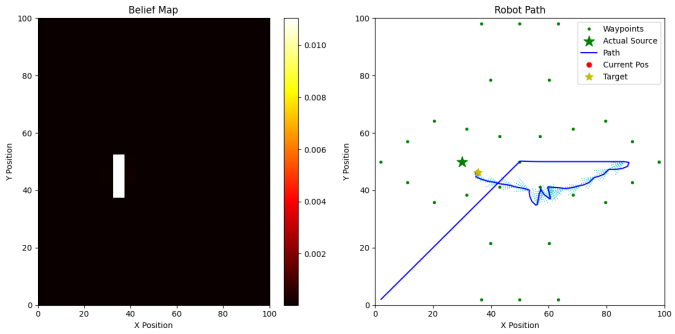

Fig. 4: Rollout algorithm-based radiation source localization for source location (30, 50)

Figure 4 represents the run of the rollout algorithm-based radiation source localization algorithm for a source located at (30, 50). The blue line represents the path taken by the drone, the blue dotted line represents the trajectory rollouts from the current position and the yellow start at the end of each algorithm-chosen trajectory endpoint position. This run localized the source at a distance of 7 meters from the actual source location.

3) Inverse Square Law Optimization: The implemented localization method is based on the inverse square law for radiation intensity and serves as a deterministic baseline for comparing different radiation source search strategies. The algorithm employs a concentric search pattern that scales automatically according to the search area consisting of three concentric circles positioned at 25%, 50%, and 75% of the search area radius. This pattern begins from the center and expands outward, with the number of measurement points per circle scaling proportionally with the map size to maintain consistent coverage across different search areas. The choice of using concentric circles for data collection is based on tests showing that other patterns, such as shamrock, were less effective in terms of coverage and accuracy. This approach balances the need to collect data covering most of the search space with the constraint of avoiding excessive time consumption.

This method localizes the radiation source by beginning with deciding the search pattern and number of measurement points on this pattern scale based on the map size. At each measurement point, the radiation sensors collect radiation count and compare it against the expected measurements based on the inverse square law, which dictates that the intensity decreases with the square distance from the source. These measurements are then weighted, assigning higher importance to stronger readings, as they indicate the proximity to the source. The collected data is fed into the Nelder-Mead optimization algorithm, which iteratively adjusts the source position and intensity by minimizing the log-space error between the expected and measured radiation counts. To handle uncertainty in source intensity, the algorithm employs multiple optimization attempts with varying initial intensity estimates (100x, 1000x, and 10000x the maximum measured count rate) to avoid local minima. The final estimated source location comes with a confidence circle, where the radius corresponds to the standard deviation of the measurements,

reflecting the level of uncertainty associated with the estimate.

Many real-world problems involve objective functions that are not differentiable due to noise, discontinuities, and radiation measurements are one of those problems. Gradient-based optimization methods struggle with such functions as they need smooth, differentiable functions to work. The Nelder-Mead algorithm is effective for non-smooth or discontinuous functions because it does not rely on gradients. Instead, it evaluates the function at simplex vertices and adjusts the simplex shape iteratively. This makes it a robust choice for optimization problems where derivative information is unavailable or unreliable. Compared to global optimization methods like evolutionary algorithms, the Nelder-Mead approach offers lower computational costs for problems with fewer variables or limited evaluations, which aligns well with the requirements of engineering optimization. [**?**]

This approach is an effective baseline for comparison due to its deterministic nature, foundation in established physics principles, reproducible behavior, and comprehensive evaluation metrics. The predefined path strategy and inverse square law optimization provide a methodical reference point against which more sophisticated, informed search strategies can be evaluated.

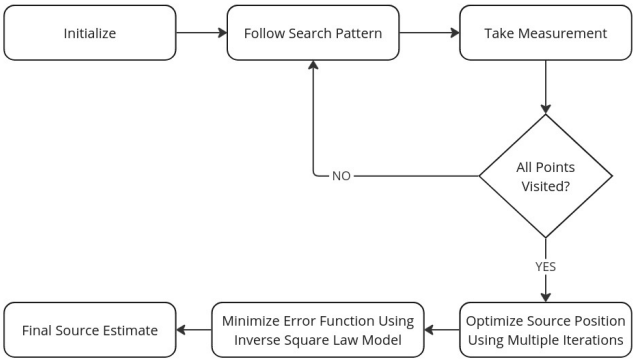

Fig. 5: Diagram of the deterministic baseline approach using concentric search patterns and Nelder-Mead optimization

Figure 5 represent the workflow of the baseline approach, from initial measurement collection through Nelder-Mead optimization and confidence circle calculation.

Figure 6 represents the run of the inverse square law optimization-based radiation source localization algorithm for a source located at (30, 50). the green ellipse represents the confidence circle around the estimated source position(green star). The red star represents the true source position, the black points represent the visited measurement points, and the blue square represents the estimated source position. This run localized the source at a distance of 7.6 meters from the actual source location.

IV. Evaluation

The efficiency of the simulation framework and the implemented algorithms were evaluated using a set of experiments. The experiments were performed randomly under a set of

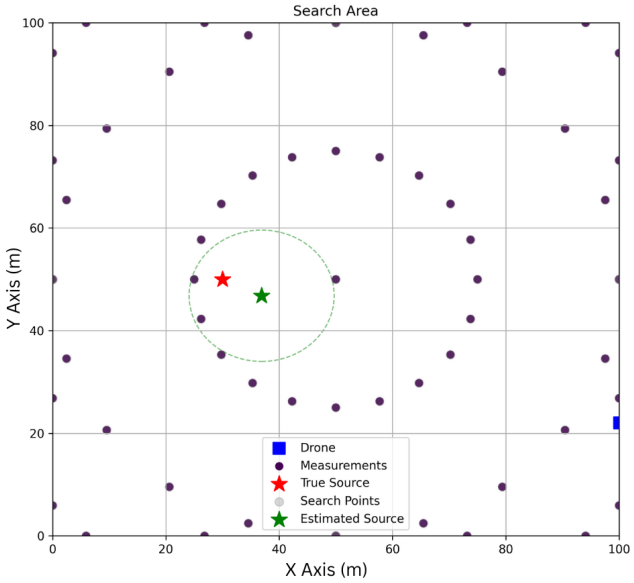

Fig. 6: inverse square optimization-based radiation source localization for source location (30, 50)

different radiation source positions. The experiments were conducted in a 100x100 meter area and the drone is assumed to take off from the origin of the area for each test. For each source position, each algorithm is tested 10 times. Each test is considered successful if the drone is able to locate a source, and the main parameters of the test will be saved into a JSON file for further analysis. The tests under the same source position are evaluated together. The evaluation metrics considered for each run are prediction error, time taken to detect the source, time taken to converge the source position, distance traveled by the drone to localize the source, number of iterations, and time taken for computation. The prediction error is calculated as the Euclidean distance between the predicted source position and the actual source position. Along with the performance metrics, the measurement history, trajectory, and computation times from each iteration are also saved for further analysis. The results of the experiments are presented in the following sections.

The tests were conducted in a 100x100 meter area with the source positioned in the following randomly selected locations: (25,80), (30,50), (50,50), (70,45), (80,70).

A. Analysis

As shown in the table I, the source location (30, 50) presents an interesting case for detailed analysis. This location was chosen for further investigation because it represents the best performance across all algorithms.

1) Prediction Error: The violin plot in Figure 8 illustrates the distribution of prediction errors across all implemented algorithms. The entropy algorithm demonstrates the widest range of performance, achieving both the highest (approximately 12 m) and lowest (approximately 2 m) prediction errors

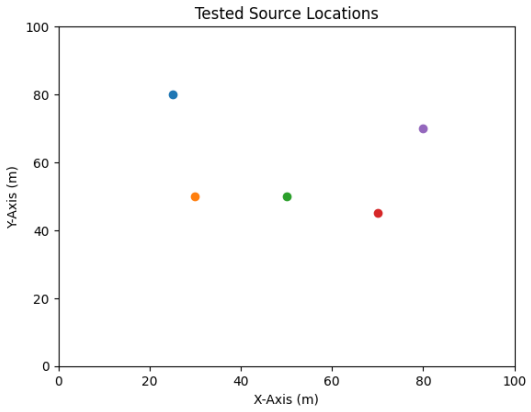

Fig. 7: Source Locations used for Evaluation

TABLE I: Algorithm Performance Comparison Across Source Locations

Location	Entropy		Rollout		Inverse Square	
	Error (m)	Time (s)	Error (m)	Time (s)	Error (m)	Time (s)
(25, 80)	6.01	125.57	10.24	177.54	14.38	415.17
(30, 50)	7.06	43.56	7.00	108.65	6.62	470.52
(50, 50)	7.21	46.12	6.89	112.45	6.83	468.24
(70, 45)	8.17	45.67	6.66	115.42	7.71	415.70
(80, 70)	8.08	61.85	6.33	91.62	4.53	431.01

Note: Error represents prediction error in meters, Time represents convergence time in seconds

TABLE II: Algorithm Performance Metrics

Metric	Entropy	Inverse Square	Rollout
Detection Time (s)	10.6763	N/A	55.3380
Total Duration (s)	43.5593	432.6485	127.6378
Total Iterations	164.4000	4886.9000	2531.6000
Total Distance	85.5140	936.5585	215.9527
Mean Computation Time (s)	0.0001	0.0001	0.0000

Note: Other performance metrics for the run at source location (30,50) that are not includeed in Table I

among all algorithms. The plot's characteristic narrowing at higher error values indicates that these larger errors occur infrequently, suggesting they are outliers rather than typical performance. Notably, the algorithm's ability to achieve the lowest prediction errors in some runs demonstrates its potential for high accuracy under favorable conditions.

The median error of the entropy algorithm is approximately 7m, which aligns with findings from previous studies by Ristic et al. [**?**] and [**?**]. In contrast, the inverse square algorithm exhibits a distinctly narrow spread, with errors consistently falling between 6 and 7.5 meters. This concentrated distribution of around 7 meters reflects the algorithm's consistency across runs, which can be attributed to its systematic measurement collection from fixed points within the search area relative to the source location.

The rollout algorithm shows prediction errors ranging from

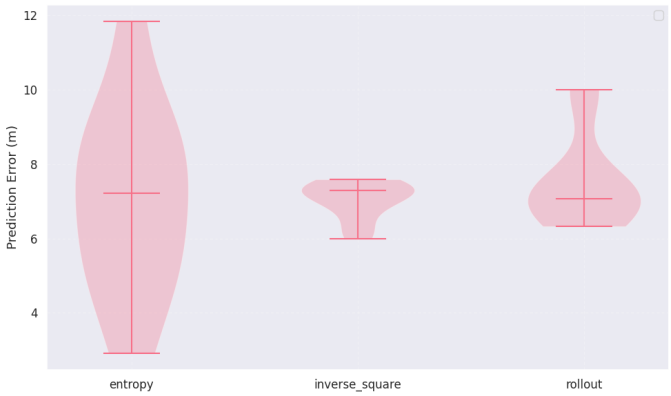

Fig. 8: Violin plot of prediction error in information-gain-based (entropy), inverse square optimization method and rollout algorithm for source location (30, 50)

6 to 10 meters, with most errors clustering around 7 meters, similar to the other algorithms. The algorithm's minimum error of 7 meters occurs frequently, which can be attributed to the chosen grid size (5 m) naturally leading to localization errors in the range of 5 to 7 meters. This pattern suggests that the grid resolution plays a significant role in determining the algorithm's precision limits.

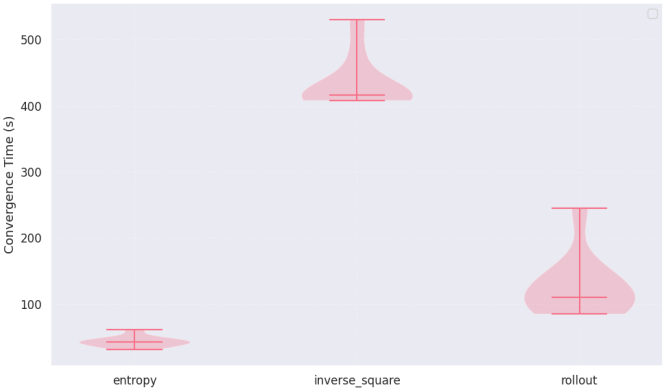

Fig. 9: Violin plot of convergence time in information-gain-based (entropy), inverse square optimization method and rollout algorithm for source location (30, 50)

2) Convergence Time:

a) Statistical Analysis: Since radiation counts follow a Poisson Distribution [**?**], non-parametric tests were selected for algorithm comparison. Specifically, the Wilcoxon Signed-Rank Test was employed to provide detailed comparisons of paired samples, accounting for both the direction and magnitude of differences. All tests were conducted at a significance level of 0.05.

b) Prediction Error Analysis: The statistical analysis of prediction errors using the Wilcoxon Signed-Rank Test revealed no significant differences between the algorithms, with detailed results presented in Table III. These findings suggest that all three algorithms achieve comparable levels of accuracy in source localization.

The pairwise comparisons revealed several key insights:

TABLE III: Wilcoxon Signed-Rank Test Results for Prediction Error

Method Comparison	Statistical Results	Performance Summary
Entropy vs. Inverse Square	Sample size: 10 Statistic (W): 26.0000 p-value: 0.9219 Effect size (r): 0.0483	Equal performance distribution with 5 samples favoring each algorithm. Negligible effect size indicates no practical difference in accuracy.
Entropy vs. Rollout	Sample size: 10 Statistic (W): 21.0000 p-value: 0.5566 Effect size (r): 0.2095	Slight advantage for Entropy (6 vs 4 samples) but small effect size and non-significant p-value indicate comparable performance.
Inverse Square vs. Rollout	Sample size: 10 Statistic (W): 19.0000 p-value: 0.4316 Effect size (r): 0.2740	Minor advantage for Inverse Square (6 vs 4 samples) but small effect size suggests minimal practical difference.

- The comparison between Entropy and Inverse Square methods showed perfect balance (5 wins each) with a negligible effect size (r = 0.0483), strongly suggesting equivalent performance.
- While Entropy showed a slight advantage over Rollout (6 vs 4 samples), the small effect size (r = 0.2095) and non-significant p-value (0.5566) indicate that this difference is not practically meaningful.
- Similarly, Inverse Square's slight advantage over Rollout (6 vs 4 samples) yielded a small effect size (r = 0.2740) and non-significant p-value (0.4316), suggesting comparable performance levels.

The consistency in non-significant results across all three comparisons, combined with small to negligible effect sizes, provides strong evidence that the algorithms achieve similar levels of prediction accuracy. This is particularly noteworthy given the balanced distribution of positive and negative ranks across comparisons, suggesting that any observed differences are likely due to random variation rather than systematic performance differences.

3) Convergence Time Analysis: The convergence time analysis utilizing the Wilcoxon Signed-Rank Test uncovered systematic performance differences among the algorithms. As demonstrated by the Figure 9 there are clear substantial differences in the time taken for convergence. The information-gain-based (entropy) algorithm consistently outperforms the inverse square optimization method and the rollout algorithm in terms of convergence time.

To validate this visual observations, the Wilcoxon Signed-Rank Test was conducted, confirming the statistical significance of the algorithms evaluated in pairs as seen in Table IV. These tests corroborate the clear performance hierarchy visible in the violin plot.

These performance differences establish a clear hierarchy among the algorithms, with the entropy-based approach demonstrating superior efficiency, followed by rollout, and then inverse square. The magnitude of these differences is substantial enough to have meaningful implications for practical applications, particularly in time-sensitive radioactive source localization tasks where rapid convergence is crucial.

TABLE IV: Wilcoxon Signed-Rank Test Results for Convergence Time

Method Comparison	Statistical Results	Performance Summary
Entropy vs. Inverse Square	Sample size: 10 Statistic (W): 0.0000 p-value: 0.0020 Effect size (r): 0.8864	Complete advantage for Entropy (10 vs 0 samples) with large effect size demonstrating clear performance superiority in convergence speed.
Entropy vs. Rollout	Sample size: 10 Statistic (W): 0.0000 p-value: 0.0020 Effect size (r): 0.8864	Complete advantage for Entropy (10 vs 0 samples) with large effect size showing consistent superior performance in convergence time.
Inverse Square vs. Rollout	Sample size: 10 Statistic (W): 0.0000 p-value: 0.0020 Effect size (r): 0.8864	Complete advantage for Rollout (10 vs 0 samples) with large effect size indicating consistently faster convergence than Inverse Square.

The consistent pattern of performance across all test cases provides strong evidence for the practical advantages of using information-theoretic approaches (entropy-based) over traditional methods in radiation source localization tasks. This finding aligns with the theoretical expectations, as the entropy-based method makes more informed decisions about measurement locations based on information gain principles.

V. Conclusions

Developing and evaluating our framework for radioactive source localization has provided valuable insights into the relative performance of different localization strategies. This method combines physics-based radiation simulation with systematic evaluation methods to compare three distinct approaches: information-gain-based and inverse square law optimization algorithms. Our experiments and evaluation across multiple source configurations demonstrate that each method can localize sources with varying efficiency and accuracy. The information-gain-based algorithm is a winner regarding convergence time and achieving the lowest position error in source localization. The algorithm while managed to achieve the lowerst position error, also experienced a few number of highest position error as visible in Figure 8. The rollout algorithm also performs well but with a slightly higher convergence time and consistently predicts a position error of around 7 meters due to the selection of a grid resolution of 5 meters. While effective, the inverse square law optimization algorithm takes significantly longer to converge and, with some source

configurations, position in this case, witnesses a higher error. It is also worth noting that the evaluation metrics are the convergence time and the position error. The convergence time also includes the movement time, and a drone with better movement control might achieve better performance in the time taken. The entropy algorithm managed to achieve the best accuracy of upto just around 2 meters, but the rollout-based method has managed to achieve around 5 meters due to the grid resolution. The inverse square law optimization method fluctuates quite significantly due to the area coverage and source position. The higher and lowest position errors in information-gain-based method represents the tradeoff between the time taken to converge and the accuracy achieved.

A. Summary

Our comprehensive evaluation of three distinct approaches to radiation source localization based on source location $(30, 50)$ in table I- information-gain-based, rollout-based, and inverse square law optimization - revealed several significant findings. Statistical analysis demonstrated that while all three methods achieved comparable accuracy in source localization, with errors ranging from 4.5 to 14.4 meters, they exhibited marked differences in convergence speed. The information-gain-based approach consistently demonstrated superior performance, achieving convergence in 43-126 seconds, followed by the rollout algorithm at 90-177 seconds. Both methods significantly outperformed the baseline inverse square method, which required 415-470 seconds for convergence.

The Wilcoxon Signed-Rank Test demonstrated significant differences in convergence times among the algorithms, with large effect sizes (r = 0.8864) supporting this finding. This statistical evidence and practical performance metrics strongly validate the effectiveness of information-theoretic methods in radiation source localization.

B. Contributions

This research makes several contributions to the field of autonomous radiation source localization. First, we have developed a physics-based simulation framework that incorporates realistic radiation behavior, including particle attenuation and scattering effects. This framework provides a reliable platform for testing and evaluating localization algorithms under controlled conditions.

Second, our implementation and comparative analysis of three distinct localization approaches establishes quantitative benchmarks for algorithm performance. The systematic evaluation methodology we developed, combining both practical performance metrics and rigorous statistical analysis, provides a framework for assessing future algorithms in this domain.

Third, our results demonstrated that, in the domain of radioactive source localization, the information-based methods could perform significantly better than the traditional predefined trajectory following methods without compromising accuracy and time. This study offers a promising direction for developing autonomous methods that may need to find radioactive sources

Fourth, we have developed a comprehensive evaluation framework with an intuitive graphical interface that enables systematic analysis of localization algorithms. This framework features built-in statistical analysis capabilities, customizable visualization tools, and an extensible architecture that facilitates easy integration of new algorithms and evaluation metrics. The framework's modular design allows researchers to incorporate additional statistical tests and performance metrics, enabling thorough comparative analysis tailored to specific research requirements.

C. Future Work

Several promising directions exist for extending and improving this research. First, the framework could be extended to handle multiple sources, which would be more challenging but more realistic. This would require extending the current methods to handle the overlapping of radiation fields. Secondly, the detection time and total time for rollout algorithm could be brought down by detecting the source at an earlier stage with lower confidence. This needs further investigation as this might lead to longer convergence times. This increase increase in convergence time could be mitigated by using a lengthier rollout step size. As it would be more ideal as the drone would not be gaining much information in smaller steps, and the large step size could help to achieve higher information gain. Thirdly, another key area for future research is implementing capabilites for tracking moving radiation sources, which wuld necessitate real-time belief updates, adaptive path planning, predictive source movement modeling, and enhanced convergence strategies for mobile targets.